

Site-specific neoatherosclerosis assessed by optical coherence tomography in patients with in-stent restenosis

Soo-Jin Kang, MD, PhD; Mineok Chang, MD; Sung-Han Yoon, MD; Jung-Min Ahn, MD; Jong-Young Lee, MD; Duk-Woo Park, MD, PhD; Seung-Whan Lee, MD, PhD; Young-Hak Kim, MD, PhD; Cheol Whan Lee, MD, PhD; Seong-Wook Park, MD, PhD; Seung-Jung Park*, MD, PhD

Department of Cardiology, University of Ulsan College of Medicine, Asan Medical Center, Seoul, South Korea

KEYWORDS

- in-stent restenosis
- neoatherosclerosis
- optical coherence tomography

Abstract

Aims: To assess the pattern of site-specific neoatherosclerosis in patients with in-stent restenosis (ISR).

Methods and results: Optical coherence tomographic (OCT) data were analysed from 146 patients with ISR (39 bare metal and 107 drug-eluting stents). Sites of in-stent minimal lumen area (MLA) were (1) bifurcation (5 mm-long segment of the proximal main branch [MB], the confluence zone and a 5 mm-long segment of the distal MB), and (2) non-bifurcation, classified as marginal (MLA within a 5 mm-long segment adjacent to the stent margin) or body (MLA confined to the stent body) type. Median stent duration was 53.7 months. In-stent MLA sites located in bifurcation segments (vs. non-bifurcation) had a higher frequency of TCFA-containing neointima (48% [23/48] vs. 27% [26/98], $p=0.015$) and thrombi (63% [30/48] vs. 36% [35/98], $p=0.003$). When in-stent MLA was located in non-bifurcation segments, TCFA-containing neointima (43% vs. 14%, $p=0.002$) and intimal rupture (45% vs. 23%, $p=0.029$) were more common in marginal vs. body types. Post-procedural CK-MB was higher in lesions whose MLA was located at bifurcation vs. non-bifurcation sites (1.8 [1.2-4.2] vs. 1.4 [0.8-2.4] ng/ml, $p=0.016$) and in marginal vs. body type (2.1 [0.9-4.4] vs. 1.2 [0.7-1.8] ng/ml, $p=0.015$). In five lesions with stent fracture, 80% of the MLA sites showed either in-stent TCFA or intimal rupture.

Conclusions: In-stent neoatherosclerosis was more common when in-stent MLA was located at bifurcation (vs. non-bifurcation), near the stent margin (vs. body), and at the stent fracture site.

Corresponding author: Asan Medical Center, 388-1 Poongnap-dong, Songpa-gu, Seoul 138-736, South Korea.

E-mail: sjpark@amc.seoul.kr

Introduction

In-stent neoatherosclerosis is an important contributing mechanism of late stent failure, such as very late stent thrombosis and in-stent restenosis (ISR), after both bare metal stent and drug-eluting stent implantation¹⁻⁵. However, the site-specific patterns of neointimal characteristics in ISR lesions still remain unclear. In native coronary artery disease, high-risk atherosclerotic plaques with a large necrotic core are prone to developing at bifurcation sites which are subject to abnormal conditions of endothelial shear stress⁶⁻⁸. Even though bifurcation stenting has been predisposed to stent thrombosis and ISR^{9,10}, the frequency and distribution of unstable neointima which develops after bifurcation stenting has not been known. The aims of this study were to use optical coherence tomography (OCT) to detect advanced neoatherosclerosis in patients with ISR and characterise the patterns of neoatherosclerosis at different sites, namely restenotic lesions located at bifurcation versus non-bifurcation sites and at stent edge versus non-edge segments.

Methods

From August 2008 to December 2013, 154 patients with ISR underwent pre-procedural OCT at the Asan Medical Center, Seoul, South Korea. Exclusion criteria were as follows: haemodynamic instability, inability of the OCT ImageWire (LightLab Imaging, Westford, MA, USA) or Dragonfly™ catheter (St. Jude Medical, St. Paul, MN, USA) to cross the lesion of restenosis into the distal vessel (owing to tight stenosis or severe vessel tortuosity), the presence of left main or saphenous vein graft lesions, acute myocardial infarction, or the presence of an angiographically visible thrombus. Before April 2011, OCT examination using the proximal occlusive technique could not be carried out in cases where the lesion was located near the ostium. OCT image analysis was performed at the Imaging Core Laboratory at Asan Medical Center. The following exclusions were made: one patient with a thrombotic coronary occlusion without significant neointima, four patients with dominant stent underexpansion and little neointima, and three patients with poor OCT images. In total, 146 patients with 146 lesions were finally included in the current analysis.

Serum creatine kinase-myocardial band (CK-MB) was measured before and after the procedure. All patients signed written, informed consent prior to the study.

The time-domain OCT procedure and its anatomical limitations for the occlusive technique in use prior to April 2011 have been previously reported^{11,12}. OCT image acquisition was performed using a commercially available system for intracoronary imaging and a 0.019 inch ImageWire (LightLab Imaging). The artery was cleared of blood by continual flush delivery, as previously described. The flush consisted of Iodixanol 370 (Visipaque™; GE Healthcare, Cork, Ireland) applied at a flow rate of 3.0 ml/s. Since April 2011, OCT images have been acquired using a non-occlusive technique and the C7XR™ system (Dragonfly™ catheter and C7XR™; LightLab Imaging [now St. Jude Medical]).

Neointima was defined as tissue formed between the luminal border and the inner border of the struts. Calcific intima was defined

as a well-delineated, signal-poor region with sharp borders. Lipidic intima was defined as a signal-poor region with diffuse borders¹³. In-stent thin-cap fibroatheroma (TCFA) was defined as a fibrous cap thickness at its thinnest part of $\leq 65 \mu\text{m}$, and an angle of lipidic tissue of $\geq 120^\circ$ inside the stent^{14,15}. Intimal rupture was determined by OCT imaging as a break in the neointima's fibrous cap enabling communication of the lumen with the underlying ruptured cavity: this definition is analogous to that of plaque rupture seen in native atherosclerotic plaques, as reported previously^{5,16}. Thrombi were defined as masses protruding into the vessel lumen, discontinuous from the surface of the vessel wall, and with a dimension $\geq 250 \mu\text{m}$. Red thrombi were characterised by high-backscattering protrusions with signal-free shadowing, whereas white thrombi were characterised by signal-rich, low-backscattering projections into the lumen^{17,18}. The axial locations of TCFA-containing intima and intimal rupture were assessed at the minimal lumen area (MLA) site (within 5 mm from the MLA frame)⁴ and within a 5 mm segment proximal and distal to the MLA site.

Bifurcation segments of the main branch (MB) consisted of a distal MB segment (5 mm-long segment distal to the carina, defined as the frame immediately distal to the take-off of the side branch), a confluence zone (confluence of MB and side branch), and a proximal MB segment (a 5 mm-long segment just above the confluence zone)¹⁹. When the in-stent MLA was located within those bifurcation segments, TCFA-containing neointima and intimal rupture were assessed at the MLA site and each of the bifurcation segments. When the in-stent MLA was located within a non-bifurcation segment, the lesions were classified as marginal or body type according to location: 1) marginal type was defined when an in-stent MLA was located within a proximal or distal 5 mm-long segment adjacent to the stent margin, and 2) body type was defined when an in-stent MLA site was confined to the body of the stent (**Figure 1**).

Stent strut coverage was assessed as previously described²⁰. All OCT parameters reported required the agreement of two observers (SJ Kang, JM Ahn).

All values are expressed as the median value (interquartile range [IQR]) or as counts and percentages (categorical variables). Continuous variables were compared by the nonparametric Mann-Whitney test; categorical variables were compared with χ^2 statistics or Fisher's exact test. All p-values were two-sided, and p-values less than 0.05 were considered to indicate statistical significance. All statistical analyses were performed using SPSS version 10.0 (SPSS Inc., Chicago, IL, USA).

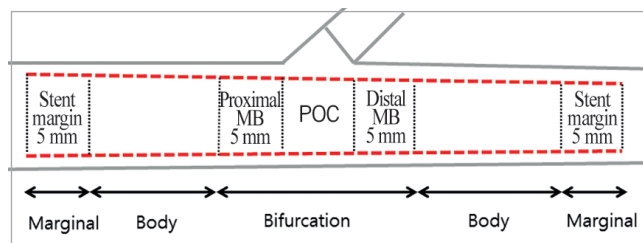


Figure 1. Definition of in-stent restenosis site.

Results

The clinical characteristics of the 146 study participants are summarised in **Table 1**. The median (IQR) follow-up time was 53.7 (18.7-87.4) months. The ISR lesions were associated with the following types of stent: 39 bare metal; 55 sirolimus-eluting (Cypher; Cordis, Johnson & Johnson, Miami Lakes, FL, USA); 23 paclitaxel-eluting (TAXUS; Boston Scientific Corp., Marlborough, MA, USA); four zotarolimus-eluting (Endeavor®; Medtronic Vascular, Santa Rosa, CA, USA); four Resolute zotarolimus-eluting (Endeavor Resolute; Medtronic Vascular); 17 everolimus-eluting (XIENCE V coronary stent system; Abbott Vascular, Santa Clara, CA, USA); two umirolium (Biolimus) A9 (Nobori; Biosensors International, Singapore); and two Cilotax™ (Cardiotec Co. Ltd, Seoul, South Korea).

Overall, in the 146 ISR lesions, MLA was 1.5 mm² (0.9-1.9 mm²). At the MLA site, TCFA-containing neointima and intimal rupture were seen in 49 (34%) lesions and 52 (36%) lesions, respectively. The MLA was located within a bifurcation segment in 48 (33%) lesions, while the remaining 98 (67%) lesions had the MLA located at a non-bifurcation segment. Overall, malapposition was observed in 23 (16%) lesions. The frequency of intraluminal thrombi was 81 (55%): red thrombi 10 (7%), white thrombi 55 (38%), and mixed thrombi 16 (11%).

In these 48 lesions, 71% of the in-stent MLA sites were located within the distal MB, 6% within the confluence zone, and 23% within the proximal MB (**Table 2, Figure 2**). The frequency of

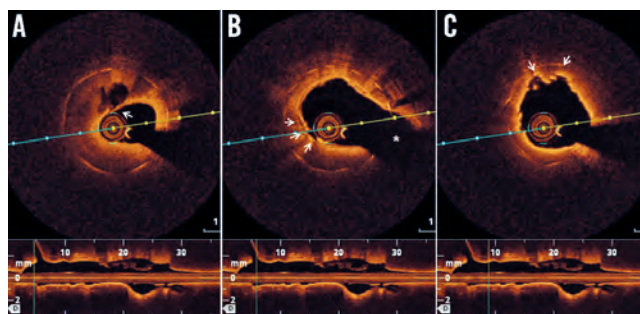


Figure 2. OCT findings in the ISR lesions at bifurcation site. A) At the MLA site within distal main branch, ruptured cavity inside the stent, ruptured TCFA (arrow) were shown. B) In-stent TCFA with disruption (arrows) was demonstrated in the confluence zone with the diagonal branch (asterisk). C) At the proximal main branch, arrows indicate TCFA-containing neointima with disruption.

TCFA-containing neointima was 52% at the distal MB, 38% at the confluence zone, and 58% at the proximal MB. The frequency of intimal rupture was 46% at the distal MB, 22% at the confluence zone and 38% at the proximal MB.

The MLA sites located within the bifurcation segments more frequently showed TCFA-containing neointima (48% [23/48] vs. 27% [26/98], $p=0.015$) and intraluminal thrombi (63% [30/48] vs. 36% [35/98], $p=0.003$) than in MLA sites located at non-bifurcation

Table 1. Baseline characteristics of the 146 patients and location of the in-stent minimal lumen area (MLA).

Variable	Total	Location of in-stent MLA		p-value
		Bifurcation	Non-bifurcation	
N	146	48	98	
Baseline clinical characteristics				
Age (years)	64.0 (56.0-69.0)	63.5 (57.2-69.0)	64 (56.0-69.0)	0.812
Male gender, n (%)	116 (80%)	39 (81%)	77 (79%)	0.829
Smoking, n (%)	76 (52%)	24 (50%)	52 (54%)	0.712
Hypertension, n (%)	97 (66%)	33 (69%)	64 (65%)	0.713
Hypercholesterolaemia, n (%)	125 (85%)	39 (81%)	86 (88%)	0.321
Diabetes mellitus, n (%)	56 (43%)	21 (44%)	35 (36%)	0.370
Previous myocardial infarction, n (%)	26 (18%)	11 (23%)	15 (15%)	0.261
Statin therapy at admission, n (%)	105 (72%)	36 (75%)	69 (71%)	0.624
Drug-eluting stent, n (%)	107 (73%)	30 (63%)	77 (79%)	0.047
Unstable angina at admission, n (%)	35 (24%)	12 (25%)	23 (24%)	0.839
High-sensitive C-reactive protein, mg/L	0.07 (0.03-0.18)	0.09 (0.04-0.22)	0.06 (0.03-0.17)	0.177
Types of vessel				
Left anterior descending, n (%)	91 (62%)	36 (75%)	55 (56%)	
Left circumflex, n (%)	9 (6%)	5 (10%)	4 (4%)	0.014
Right coronary, n (%)	45 (31%)	7 (15%)	38 (39%)	
Left main, n (%)	1 (1%)	0 (0%)	1 (1%)	
Total stent length, mm	28.0 (17.8-51.0)	30.0 (18.0-50.3)	28.0 (16.0-51.3)	0.741
Stent duration, months	53.7 (18.7-87.4)	74.9 (39.9-108.8)	48.8 (15.8-80.3)	0.012
Values are median (interquartile range) or n (%).				

Table 2. OCT findings in the 48 lesions in which in-stent MLA was located within bifurcation segments.

At the MLA site	
Location of MLA	
Distal main branch, n (%)	34 (71%)
Confluence zone, n (%)	3 (6%)
Proximal main branch, n (%)	11 (23%)
MLA, mm ²	1.5 (1.0-1.9)
Lipid neointima, n (%)	45 (94%)
Intimal rupture, n (%)	20 (42%)
In-stent TCFA, n (%)	23 (48%)
5 mm-long segment proximal to the MLA	
Intimal rupture, n (%)	21 (44%)
In-stent TCFA, n (%)	33 (68%)
5 mm-long segment distal to the MLA	
Intimal rupture, n (%)	11 (23%)
In-stent TCFA, n (%)	19 (40%)
Thrombi within in-stent segment, n (%)	30 (63%)
Calcification within in-stent segment, n (%)	11 (23%)

Values are median (interquartile range) for continuous variables or n (%). MLA: minimal lumen area; OCT: optical coherence tomography; TCFA: thin-cap fibroatheroma

segments. Among the 23 lesions with TCFA at the MLA site, the TCFA was distributed at the flow divider in five (22%) lesions, at the lateral wall in nine (39%) lesions, and at both the flow divider and the lateral wall in nine (39%) lesions. TCFA-containing neointima (68% vs. 40%) and intimal rupture (44% vs. 23%) were more frequently observed in 5 mm-long segments proximal (vs. distal) to the MLA site (all $p < 0.05$).

In the 98 lesions in which MLA was located at a non-bifurcation segment, 42 lesions were classified as marginal type and 56 lesions as body type (Figure 3). At the MLA site, TCFA-containing neointima and intimal rupture were found more frequently in marginal vs. body type (Table 3, Figure 4).

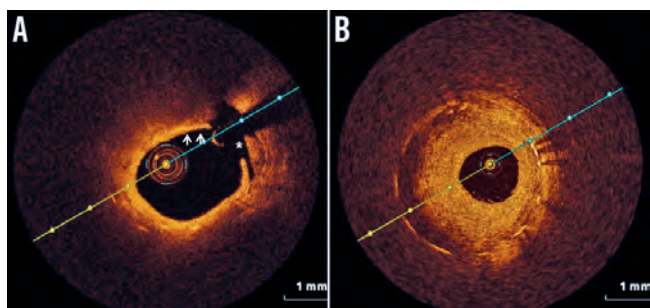


Figure 3. OCT findings in the ISR lesions at non-bifurcation site. A) Marginal type (MLA site located within 5 mm in-stent segment adjacent to the proximal stent edge). Intimal rupture (asterisk) and TCFA (arrows) were shown. B) Body type (MLA site confined to the stent body portion).

Table 3. OCT findings in the 98 lesions in which in-stent MLA was located at non-bifurcation segments.

N	Marginal type	Body type	p-value
	42	56	
In-stent thrombi, n (%)	21 (50%)	14 (25%)	0.018
In-stent calcification, n (%)	5 (12%)	5 (9%)	0.505
Lipid neointima, n (%)	39 (93%)	52 (93%)	1.000
At the MLA site			
MLA, mm ²	1.5 (0.9-1.8)	1.4 (0.9-1.9)	1.000
Intimal rupture, n (%)	19 (45%)	13 (23%)	0.029
In-stent TCFA, n (%)	18 (43%)	8 (14%)	0.002
5 mm in-stent segment adjacent to the stent margin			
Intimal rupture, n (%)	19 (45%)		
In-stent TCFA, n (%)	18 (43%)		
5 mm reference segment			
Plaque rupture, n (%)	6 (14%)		
TCFA, n (%)	8 (19%)		
5 mm in-stent segment proximal to the MLA			
Intimal rupture, n (%)		3 (5%)	
In-stent TCFA, n (%)		7 (13%)	
5 mm in-stent segment distal to the MLA			
Intimal rupture, n (%)		2 (4%)	
In-stent TCFA, n (%)		7 (13%)	

Values are median (interquartile range) or n (%). MLA: minimal lumen area; TCFA: thin-cap fibroatheroma

In five lesions, the MLA site was associated with stent fracture. All five affected stents were located in right coronary arteries, the specific fracture site being either stent body (n=4 lesions) or the proximal MB of the bifurcation segment (n=1 lesion). At the MLA site, four (80%) lesions showed in-stent TCFA (n=2) or intimal rupture (n=2). TCFA-containing neointima proximal to the MLA was seen in two (40%) lesions.

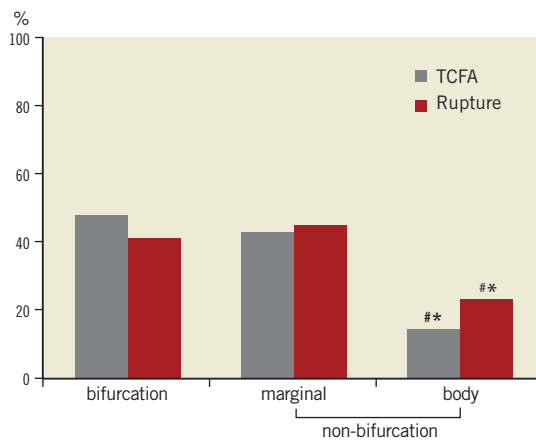


Figure 4. Frequencies of in-stent TCFA and intimal rupture according to the location of in-stent MLA. (# p-value < 0.05 vs. bifurcation, * p-value < 0.05 vs. marginal type)

All patients underwent repeat revascularisation for the treatment of their ISR lesions. Although pre-procedural peak CK-MB was similar (1.0 ng/ml [0.4-1.7 ng/ml] vs. 0.9 ng/ml [0.6-2.2 ng/ml], $p=0.8$), post-procedural CK-MB was significantly higher in ISR lesions whose MLA was located within a bifurcation segment as compared to a non-bifurcation segment (1.8 ng/ml [1.2-4.2 ng/ml] vs. 1.4 ng/ml [0.8-2.4 ng/ml], $p=0.016$). Among the lesions in which the MLA was located within a non-bifurcation, the post-procedural CK-MB was much higher in marginal-type ISR lesions compared with those in body type (2.1 ng/ml [0.9-4.4 ng/ml] vs. 1.2 ng/ml [0.7-1.8 ng/ml], $p=0.015$).

Post-procedure, TIMI <3 was shown in 11 lesions, which included five (45%) lesions with ISR at a bifurcation and three (27%) lesions with a marginal type of ISR. Seven (64%) of the 11 lesions showed in-stent TCFA or rupture.

Discussion

The major findings of this OCT study in patients with ISR are the following. 1) In-stent MLA sites were more likely to have TCFA-containing neointima and intraluminal thrombi when the MLA was located within bifurcation (vs. non-bifurcation). 2) When in-stent MLA was located within a non-bifurcation segment, TCFA-containing neointima and intimal rupture were more frequent in marginal-type (in-stent MLA within a 5 mm-long segment adjacent to the stent margin) compared to body-type (MLA site confined to the body) lesions. 3) Post-procedural CK-MB was significantly higher in the lesions whose MLA was located within bifurcation (vs. non-bifurcation) segments and also in those lesions classified as marginal (vs. body) type.

Previous studies showed that abnormal endothelial shear stress is associated with differential distribution of high-risk, rupture-prone plaques along the native coronary artery⁶⁻⁸. Bifurcations, inherently geometrically complex regions, generate disturbed laminar flow and abnormal wall shear stress patterns that have the potential to play a role in plaque accumulation and destabilisation^{8,21,22}. Additionally, it has been suggested that atherosclerotic plaques at coronary artery bifurcations have a heterogeneous nature, depending on their anatomical location and the segment involved²³.

With constant exposure to turbulent blood flow and excessive shear stress, stents at bifurcations are predisposed to thrombus formation and ISR^{9,10}. The degree of neointimal growth and vascular inflammation following stent implantation correlates inversely with wall shear stress²⁴⁻²⁶. In a recent computational simulation study, measurements of wall shear stress and blood stagnation (relative residence time) showed that wall regions were more prone to the risk of restenosis if they were located next to stent struts and to bifurcations²⁷. Our current study demonstrated that neointimal growth has characteristics specific to the site of ISR. Advanced neointimal growth, such as TCFA-containing neointima and intimal rupture, developed more frequently when the MLA of the ISR lesion was located at the bifurcation or adjacent to the stent margin. Pathological and *in vivo* imaging studies showed that in-stent neointimal growth makes an important contribution to the failure

of bare metal or drug-eluting stents by, for example, very late stent thrombosis or late ISR¹⁻⁵. The site-specific progression of neointimal atherosclerosis may contribute to the particularly high risk of stent thrombosis and restenosis after bifurcation stenting. Stent duration was much longer when lesions with ISR were located at bifurcation vs. non-bifurcation sites (74.9 [39.9-108.8] vs. 48.8 [15.8-80.3] months, $p=0.012$). Neointimal atherosclerosis progresses over time, such that the development of vulnerable neointima and ISR at bifurcation points is likely to increase with time after stent implantation under continuous exposure to wall shear stress.

The mechanism of edge vascular response and edge restenosis has been considered multifactorial. Disruption of *de novo* atherosclerotic change in stented segments and reference segments may lead to edge restenosis as well as stent thrombosis²⁸. Mechanical stress determined by angulation or calcification at the edge segment and biomechanical properties of the DES may cause chronic local inflammation, neointimal overgrowth and edge ISR²⁹. The mechanism and impact of a higher rate of in-stent neointimal atherosclerosis at the stent margin needs to be clarified in further studies.

Ali et al reported that vulnerable neointima formation and post-procedural CK-MB elevation was greater in lesions associated with DES compared with bare metal stents, suggesting that neointimal atherosclerosis has an impact on distal embolisation and periprocedural MI³⁰. In the current study, the high level of CK-MB post-stenting following treatment of ISR at bifurcation sites or near the stent margin may be partly explained by the presence of advanced neointimal atherosclerosis at those sites.

Nakazawa et al suggested that stent fracture was frequently associated with adverse pathological findings, such as restenosis and stent thrombosis³¹. In addition, Kashiwagi et al showed that intimal hyperplasia is enhanced at the fracture site. Loss of ability to scaffold the artery wall against mechanical stress and failure of local drug delivery may be related to excessive intimal growth at the fracture site³².

Limitations

This study had several limitations. First, owing to its relatively small sample size, OCT characteristics of neointima were not compared within the various types of DES implanted. Second, clinical outcomes after treatment of ISR lesions were not reported. Third, attenuation caused by large amounts of red thrombus might have obscured the underlying neointima morphology, potentially leading to an underestimation of the frequencies of TCFA-containing neointima and intimal rupture. Although the side branch ostium is the most common site of ISR after bifurcation stenting, it was not assessed by side branch pullback OCT. Even though patients who required dilation prior to OCT imaging were systematically excluded, we cannot rule out the possibility that the OCT procedure may have contributed to some of the findings, such as neointimal disruption.

Conclusions

In-stent neointimal atherosclerosis was more common when in-stent MLA was located at the bifurcation (vs. non-bifurcation), near the stent margin (vs. body), and at the stent fracture site.

Impact on daily practice

Neoatherosclerosis has been one of the important mechanisms of late stent failure. In the current study, in-stent TCFA and intimal rupture were more common when in-stent restenosis was located at the bifurcation, stent margin and stent fracture sites. These findings may explain the higher rate of restenosis and stent thrombosis after stent implantation at those sites. Site-specific advanced neoatherosclerosis may contribute to the high risk of periprocedural myocardial infarction during target lesion revascularisation.

Acknowledgements

This study was supported by a grant from the Korea Health 21 R&D Project, Ministry of Health and Welfare, Korea (A090264).

Conflict of interest statement

The authors have no conflicts of interest to declare.

References

1. Nakazawa G, Otsuka F, Nakano M, Vorpahl M, Yazdani SK, Ladich E, Kolodgie FD, Finn AV, Virmani R. The pathology of neoatherosclerosis in human coronary implants bare-metal and drug-eluting stents. *J Am Coll Cardiol*. 2011;57:1314-22.
2. Nakazawa G, Vorpahl M, Finn AV, Narula J, Virmani R. One step forward and two steps back with drug-eluting-stents: from preventing restenosis to causing late thrombosis and nouveau atherosclerosis. *JACC Cardiovasc Imaging*. 2009;2:625-8.
3. Takano M, Yamamoto M, Inami S, Murakami D, Ohba T, Seino Y, Mizuno K. Appearance of lipid-laden intima and neovascularization after implantation of bare-metal stents extended late-phase observation by intracoronary optical coherence tomography. *J Am Coll Cardiol*. 2009;55:26-32.
4. Kang SJ, Mintz GS, Akasaka T, Park DW, Lee JY, Kim WJ, Lee SW, Kim YH, Whan Lee C, Park SW, Park SJ. Optical coherence tomographic analysis of in-stent neoatherosclerosis after drug-eluting stent implantation. *Circulation*. 2011;123:2954-63.
5. Kang SJ, Mintz GS, Park DW, Lee SW, Kim YH, Lee CW, Han KH, Kim JJ, Park SW, Park SJ. Tissue characterization of in-stent neointima using intravascular ultrasound radiofrequency data analysis. *Am J Cardiol*. 2010;106:1561-5.
6. Virmani R, Burke AP, Farb A, Kolodgie FD. Pathology of the vulnerable plaque. *J Am Coll Cardiol*. 2006;47:C13-8.
7. Waksman R, Serruys PW, Schaar J, editors. The Vulnerable Plaque. Second edition. London, UK: Informa Healthcare, 2007: p.13-27.
8. Slager CJ, Wentzel JJ, Gijsen FJ, Schuurbijs JC, van der Wal AC, van der Steen AF, Serruys PW. The role of shear stress in the generation of rupture-prone vulnerable plaques. *Nat Clin Pract Cardiovasc Med*. 2005;2:401-7.
9. Al Suwaidi J, Berger PB, Rihal CS, Garratt KN, Bell MR, Ting HH, Bresnahan JF, Grill DE, Holmes DR Jr. Immediate and long-term outcome of intracoronary stent implantation for true bifurcation lesions. *J Am Coll Cardiol*. 2000;35:929-36.
10. Iakovou I, Schmidt T, Bonizzoni E, Ge L, Sangiorgi GM, Stankovic G, Airoldi F, Chieffo A, Montorfano M, Carlino M, Michev I, Corvaja N, Briguori C, Gerckens U, Grube E, Colombo A. Incidence, predictors, and outcome of thrombosis after successful implantation of drug-eluting stents. *JAMA*. 2005;293:2126-30.
11. Gonzalo N, Garcia-Garcia HM, Regar E, Barlis P, Wentzel J, Onuma Y, Ligthart J, Serruys PW. In vivo assessment of high-risk coronary plaques at bifurcations with combined intravascular ultrasound virtual histology and optical coherence tomography. *JACC Cardiovasc Imaging*. 2009;2:473-82.
12. Xie Y, Takano M, Murakami D, Yamamoto M, Okamoto K, Inami S, Seimiya K, Ohba T, Seino Y, Mizuno K. Comparison of neointimal coverage by optical coherence tomography of a sirolimus-eluting stent versus a bare metal stent three months after implantation. *Am J Cardiol*. 2008;102:27-31.
13. Yabushita H, Bouma BE, Houser SL, Aretz HT, Jang IK, Schlendorf KH, Kauffman CR, Shishkov M, Kang DH, Halpern EF, Tearney GJ. Characterization of human atherosclerosis by optical coherence tomography. *Circulation*. 2002;106:1640-5.
14. Regar E, van Beusekom HM, van der Giessen WJ, Serruys PW. Images in cardiovascular medicine. Optical coherence tomography findings at 5-year follow-up after coronary stent implantation. *Circulation*. 2005;112:e345-6.
15. Habara M, Terashima M, Nasu K, Kaneda H, Inoue K, Ito T, Kamikawa S, Kurita T, Tanaka N, Kimura M, Kinoshita Y, Tsuchikane E, Matsuo H, Ueno K, Katoh O, Suzuki T. Difference of tissue characteristics between early and very late restenosis lesions after bare-metal stent implantation: an optical coherence tomography study. *Circ Cardiovasc Interv*. 2011;4:232-8.
16. Prati F, Regar E, Mintz GS, Arbustini E, Di Mario C, Jang IK, Akasaka T, Costa M, Guagliumi G, Grube E, Ozaki Y, Pinto F, Serruys PW; Expert's OCT Review Document. Expert review document on methodology, terminology, and clinical applications of optical coherence tomography: physical principles, methodology of image acquisition, and clinical application for assessment of coronary arteries and atherosclerosis. *Eur Heart J*. 2010;31:401-15.
17. Kume T, Akasaka T, Kawamoto T, Ogasawara Y, Watanabe N, Toyota E, Neishi Y, Sukmawan R, Sadahira Y, Yoshida K. Assessment of coronary arterial thrombus by optical coherence tomography. *Am J Cardiol*. 2006;97:1713-7.
18. Jang IK, Tearney GJ, MacNeill B, Takano M, Moselewski F, Iftima N, Shishkov M, Houser S, Aretz HT, Halpern EF, Bouma BE. In vivo characterization of coronary atherosclerotic plaque by use of optical coherence tomography. *Circulation*. 2005;111:1551-5.
19. Rodriguez-Granillo GA, Garcia-Garcia HM, Wentzel J, Valgimigli M, Tsuchida K, van der Giessen W, de Jaegere P, Regar E, de Feyter PJ, Serruys PW. Plaque composition and its relationship with acknowledged shear stress patterns in coronary arteries. *J Am Coll Cardiol*. 2006;47:884-5.
20. Gonzalo N, Barlis P, Serruys PW, Garcia-Garcia HM, Onuma Y, Ligthart J, Regar E. Incomplete stent apposition and delayed tissue coverage are more frequent in drug-eluting stents implanted during primary percutaneous coronary intervention

for ST-segment elevation myocardial infarction than in drug-eluting stents implanted for stable/unstable angina: insights from optical coherence tomography. *JACC Cardiovasc Interv.* 2009;2:445-52.

21. Malek AM, Alper SL, Izumo S. Hemodynamic shear stress and its role in atherosclerosis. *JAMA.* 1999;282:2035-42.

22. Asakura T, Karino T. Flow patterns and spatial distribution of atherosclerotic lesions in human coronary arteries. *Circ Res.* 1990;66:1045-66.

23. Han SH, Puma J, García-García HM, Nasu K, Margolis P, Leon MB, Lerman A. Tissue characterisation of atherosclerotic plaque in coronary artery bifurcations: an intravascular ultrasound radiofrequency data analysis in humans. *EuroIntervention.* 2010;6:313-20.

24. Papafaklis MI, Bourantas CV, Theodorakis PE, Katsouras CS, Naka KK, Fotiadis DI, Michalis LK. The effect of shear stress on neointimal response following sirolimus- and paclitaxel-eluting stent implantation compared with bare-metal stents in humans. *JACC Cardiovasc Interv.* 2010;3:1181-9.

25. Wentzel JJ, Krams R, Schuurbijs JC, Oomen JA, Kloet J, van Der Giessen WJ, Serruys PW, Slager CJ. Relationship between neointimal thickness and shear stress after Wallstent implantation in human coronary arteries. *Circulation.* 2001;103:1740-5.

26. Carlier SG, van Damme LC, Blommerde CP, Wentzel JJ, van Langehove G, Verheye S, Kockx MM, Knaapen MW, Cheng C, Gijssen F, Duncker DJ, Stergiopoulos N, Slager CJ, Serruys PW, Krams R. Augmentation of wall shear stress inhibits neointimal hyperplasia after stent implantation: inhibition through reduction of inflammation? *Circulation.* 2003;107:2741-6.

27. Chiastra C, Morlacchi S, Gallo D, Morbiducci U, Cárdenes R, Larrabide I, Migliavacca F. Computational fluid dynamic simulations of image-based stented coronary bifurcation models. *J R Soc Interface.* 2013;10:20130193.

28. Gogas BD, Garcia-Garcia HM, Onuma Y, Muramatsu T, Farooq V, Bourantas CV, Serruys PW. Edge vascular response after percutaneous coronary intervention: an intracoronary ultrasound and optical coherence tomography appraisal: from radioactive platforms to first- and second-generation drug-eluting stents and bioresorbable scaffolds. *JACC Cardiovasc Interv.* 2013;6:211-21.

29. Kim YG, Oh IY, Kwon YW, Han JK, Yang HM, Park KW, Lee HY, Kang HJ, Koo BK, Kim HS. Mechanism of edge restenosis after drug-eluting stent implantation. Angulation at the edge and mechanical properties of the stent. *Circ J.* 2013;77:2928-35.

30. Ali ZA, Roleder T, Narula J, Mohanty BD, Baber U, Kovacic JC, Mintz GS, Otsuka F, Pan S, Virmani R, Sharma SK, Moreno P, Kini AS. Increased thin-cap neoatheroma and periprocedural myocardial infarction in drug-eluting stent restenosis: multimodality intravascular imaging of drug-eluting and bare-metal stents. *Circ Cardiovasc Interv.* 2013;6:507-17.

31. Nakazawa G, Finn AV, Vorpahl M, Ladich E, Kutys R, Balazs I, Kolodgie FD, Virmani R. Incidence and predictors of drug-eluting stent fracture in human coronary artery a pathologic analysis. *J Am Coll Cardiol.* 2009;54:1924-31.

32. Kashiwagi M, Tanaka A, Kitabata H, Ino Y, Tsujioka H, Komukai K, Ozaki Y, Ishibashi K, Tanimoto T, Takarada S, Kubo T, Hirata K, Mizukoshi M, Imanishi T, Akasaka T. OCT-verified neointimal hyperplasia is increased at fracture site in drug-eluting stents. *JACC Cardiovasc Imaging.* 2012;5:232-3.